GEOPHYSICAL RESEARCH LETTERS, VOL. 23, NO. 20, PAGES 2819-2822, OCTOBER 1, 1996

Micromagnetic modeling of Bloch walls with Néel caps in magnetite

Song Xu[1] and David J. Dunlop

Physics, Erindale College, University of Toronto, Mississauga, Ontario, Canada

Abstract. Two-dimensional micromagnetic modeling of 180° domain walls in magnetite predicts that at depths >0.07 μm below the surface, the walls are Bloch-like, with spins rotating in the plane of the wall in order to eliminate magnetic poles on the wall and reduce demagnetizing energy, E_d. The Bloch wall width is ≈0.16 μm, in agreement with magnetic force microscope (MFM) data. Near a crystal boundary, the walls are Néel-like: spins rotate in the plane of the surface in order to eliminate surface poles. This Néel cap is ≈0.3 μm wide and is offset with respect to the underlying Bloch wall. The Néel cap is narrower and shallower in magnetite (relative to Bloch wall width) than in iron, mainly because E_d is not as overwhelmingly important compared to other energies in magnetite as it is in iron. As a consequence of the smaller Néel cap in magnetite, the surface field produced by a domain wall is due mainly to the underlying Bloch wall, with only a minor contribution from the Néel cap. This prediction is consistent with MFM imaging of domain walls on free surfaces of magnetite crystals.

Bloch and Néel Walls

Classical domain theory predicts magnetic domain walls of two basic types, Bloch and Néel (Landau and Lifschitz, 1935; Néel, 1944, 1956). In a 180° Bloch wall separating antiparallel domains, the $\mathbf{M_s}$ vector rotates through 180° in the plane of the wall and no magnetic poles appear on or within the wall (Figure 1b). However, poles do appear where the Bloch wall intersects the crystal surface. For the most favourable viewing of domain structures in magnetite, the crystal is cut and polished parallel to {110} which contains two sets of <111> magnetocrystalline easy axes (Özdemir et al., 1995). The density of surface poles on the {110} viewing surface at the termination of a Bloch wall is $\mathbf{M_s}\cdot\hat{\mathbf{n}}$, where $\hat{\mathbf{n}}$ is the surface normal.

These surface poles generate a demagnetizing energy, E_d. The surface poles can be eliminated if $\mathbf{M_s}$ rotates in the plane of the surface rather than in the plane of the wall (Figure 1a). Such a structure is called a Néel wall, and is typical of thin films with a large surface/volume ratio. Although Néel walls eliminate poles on the crystal surface, they generate volume poles within the wall with a density $\nabla\cdot\mathbf{M_s}$ ($= \partial M_{sy}/\partial y$ if y is the direction perpendicular to the wall). These poles are of opposite sign in the two halves of the wall.

The Néel-wall volume poles create a demagnetizing energy E_d which is greater than E_d of the Bloch-wall surface poles if the Néel wall extends to any great depth in the crystal. Using the results of Lilley (1950), we have calculated energies per unit area for Bloch and Néel walls parallel to (110) in bulk magnetite. The results are normalized to $(A|K_1|)^{1/2}$, where A is exchange constant and K_1 is first-order magnetocrystalline anisotropy constant. If only the exchange energy E_e and magnetocrystalline anisotropy energy E_a are considered, the energies are 1.88 for Bloch walls and 1.83 for Néel walls. When demagnetizing energy E_d is included, the Bloch-wall energy is unchanged (since surface effects are ignored in the bulk calculation) but the Neel-wall energy increases to 13.4.

Thus except in thin films, we would expect walls to be a hybrid of Bloch and Néel types, with the Bloch structure dominant in the crystal interior and the Néel structure appearing close to the surface (e.g., LaBonte, 1969). The expected near-surface structure is often called a *Néel cap* because it should extend only to a shallow depth in the crystal (e.g., Schcinfein ct al., 1991).

Magnetic Force Microscope Profiles

With the magnetic force microscope or MFM, it is now possible to measure directly the magnetic fields created by Néel and Bloch walls in nanoscale traverses over the crystal surface. The MFM typically responds to the second derivative of vertical field, d^2H_z/dz^2 (Williams et al., 1992; Proksch et al., 1994). Using the results of Sharma (1966) for the magnetic field $\mathbf{H}$ produced by a uniformly magnetized rectangular body, we have calculated profiles expected over walls with purely Néel and Bloch structure, respectively (Figure 2). Sharma's results are easily extended to infinite rectangular rods, which are the modeling elements in our micromagnetic calculations below.

The Néel wall has an antisymmetric profile in Figure 2, because the volume pole density is positive in one half of the wall and negative in the other half (Figure 1a). The Bloch wall has a symmetric profile, because surface poles of a single sign appear at the surface intersection of the wall (Figure 1b). For the best

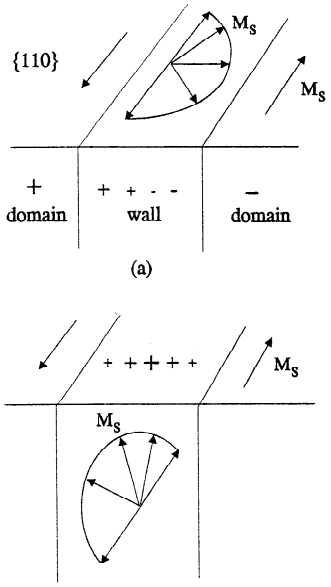

Figure 1. Rotation of the $\mathbf{M_s}$ vector across (a) a Néel wall or (b) a Bloch wall between antiparallel domains. Positive and negative magnetic poles are denoted by + and - signs.

[1]Now at Mountain Lake Software, Toronto, Canada

Paper number 96GL01568
0094-8534/96/96GL-01568$05.00

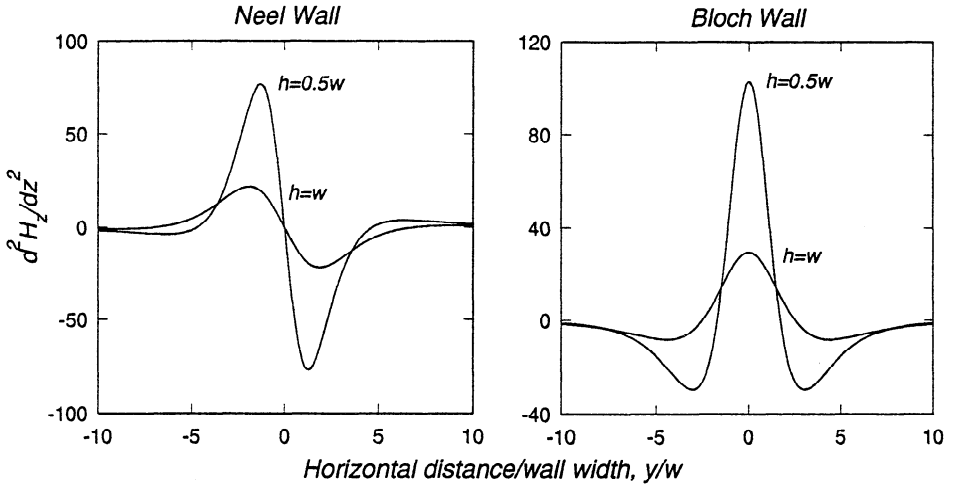

Figure 2. Surface profiles of d^2H_z/dz^2 over Néel and Bloch walls. The distance above the surface is h.

resolution of wall width and structure, the scan height h should ideally be ≤0.5w. Resolution is much poorer when h≥w.

Micromagnetic Model

We have carried out 2-dimensional micromagnetic modeling to determine the exact structures and surface field profiles of 180° walls in magnetite. In similar modeling for iron, Scheinfein et al. (1991) found an offset Néel cap wider than the Bloch wall below. Taking these results as a guide, we concentrated our modeling elements within 5-10 wall widths below the free surface and on either side of the expected Bloch wall center. We assumed that at depth in the crystal, the wall has ideal Bloch structure and that at many wall widths, the domains have uniform $\mathbf{M}_s$ (see Figure 3).

The modeling region was 1.2 μm wide and 0.8 μm deep, and was divided into 120 by 80 cells. Each cell measured 10 nm × 10 nm, ≈1/10th of the expected Bloch wall width, w. In the micromagnetic calculation, the orientations of the $\mathbf{M}_s$ vectors of the 120 × 80 cells were varied iteratively until the sum of the exchange energy, E_e, the crystalline anisotropy energy, E_a, and the demagnetizing energy, E_d, was minimized. Expressions for E_e, E_a and E_d and details of the minimization procedure are given by Xu et al. (1994). Efficient methods of evaluating E_d are essential in micromagnetic calculations (Yuan and Bertram, 1992; Berkov et al., 1993; Fabian et al., 1996).

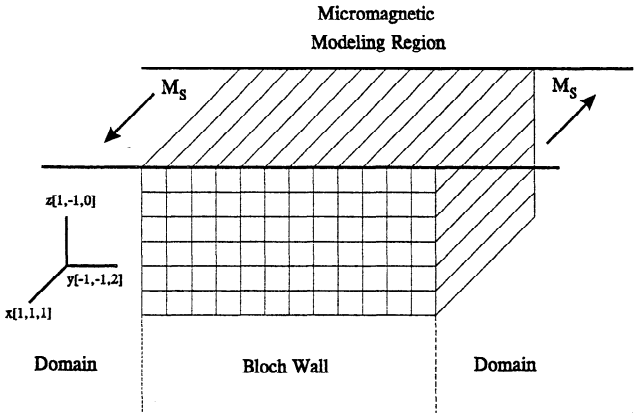

Figure 3. The array of cells used in micromagnetic modeling relative to the domains and underlying Bloch wall. $\mathbf{M}_s$ is fixed in the two domains; $\mathbf{M}_s$ in the Bloch wall region varies according to eqn. (1).

Our formulation is an outgrowth of the work of Newell et al. (1993). Calculations were carried out using a KSR1 parallel-processor computer.

The initial structure from which the iteration started, which was also the boundary condition at depth, was a 1-dimensional Bloch wall:

$$M_x(y) = M_s \tanh[y/(A/|K_1|)^{1/2}], \quad M_z(y) = M_s \operatorname{sech}[y/(A/|K_1|)^{1/2}]. \quad (1)$$

The material constants used were M_s= 480 kA/m, K_1= −12.5 kJ/m^3 and A= 1.32 × 10^{-11} J/m. The $\mathbf{M}_s$ vectors in domains 1 and 2 were in $[1\,1\,1]$ and $[\bar{1}\,\bar{1}\,\bar{1}]$ crystalline easy directions, respectively, and the top viewing surface was $(1\,\bar{1}\,0)$. Thus the Cartesian axes in Figure 3 relative to the crystallographic axes are x: $[1\,1\,1]$; y (normal to the wall): $[\bar{1}\,\bar{1}\,2]$; z (normal to the viewing surface): $[1\,\bar{1}\,0]$.

Calculated Structures

The calculated structure of a 180° wall in the y-z plane is shown in Figure 4. The x-y surface, on which domains would be viewed and MFM profiles measured, is seen edge on at the top. Each arrow plotted is the projection of the $\mathbf{M}_s$ vector on the y-z plane and represents an average of the $\mathbf{M}_s$ directions in four adjacent cells.

Within the domains, the $\mathbf{M}_s$ vector is perpendicular to the plane of the page, as indicated by a small dot marking the head or tail of each vector and the ⊗, ⊙ symbols. At depth, the wall is Bloch-like, with $\mathbf{M}_s$ rotating in the plane of the wall. In the middle of the Bloch wall, $\mathbf{M}_s$ is nearly parallel to −z and thus appears full scale in the figure. To either side, $\mathbf{M}_s$ has a component into or out of the page, and so its in-page component (the arrow plotted) is reduced.

The Bloch wall is about 16 cell widths or 160 nm (0.16 μm) wide. This estimate of w is in fair agreement with the conventional width given by domain theory (e.g., Kittel, 1949), which is $\sim\pi(A/|K_1|)^{1/2} \approx$ 100 nm or 0.1 μm for magnetite.

Within the top 70 nm (about one-half of w) below the free surface, the spins turn over to be surface-parallel. As in iron (Scheinfein et al., 1991), the Néel cap in magnetite is wider than the Bloch wall below and is quite strongly offset to one side.

The offset facilitates flux linkage with the underlying Bloch wall. The offset Néel cap forms part of an extended flux loop, completed by the left part of the Bloch wall at depth and a return or "ascending arm" of similar width to the left of the Bloch wall. The $\mathbf{M}_s$ vectors in the return column are basically perpendicular to the page but have

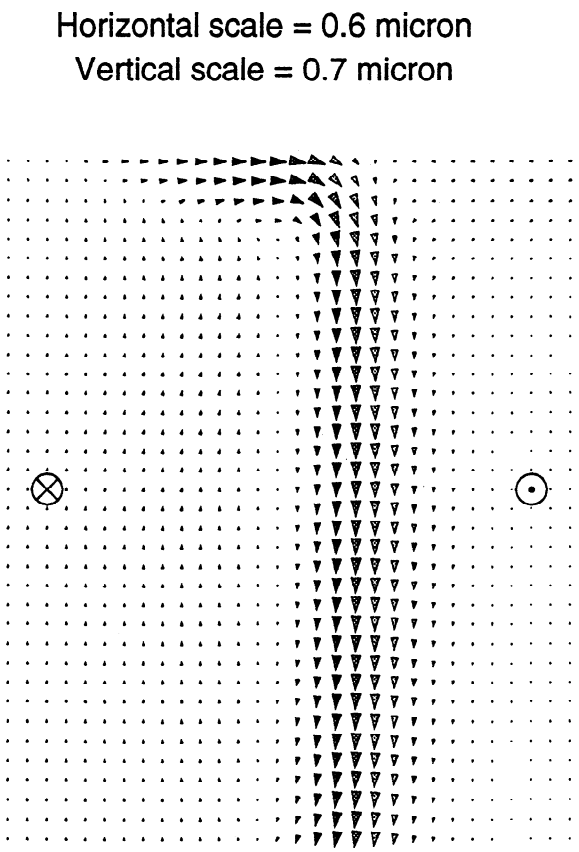

Figure 4. A cross-section through part of the modeled region, showing the fine structure of the 180° wall: a Néel cap at the free surface (top), a Bloch wall at depth, and a return flux column of similar width to the Bloch wall located to the left of the wall. Each arrow represents the component of $\mathbf{M}_s$ in the y-z plane of section, averaged over 4 adjacent cells (only 1 cell in 4 is shown). Vectors into and out of the page are denoted by ⊗, ⊙.

a small upward component. Similarly the $\mathbf{M}_s$ vectors in the Bloch wall are basically in the plane of the wall but have a small component to the left. Although the Néel cap is surficial and represents a concentration of flux, the rest of the flux loop is distributed over a much greater depth range, and is actually most obvious near the bottom of the modeled region.

Simulated MFM Profiles

Profiles representing MFM response, i.e., vertical gradient of the magnetic force between the magnetized tip of the MFM cantilever and the field **H** due to the magnetization structure of the modeled "sample" below, were calculated by the same method as in Figure 2, except that the width of the MFM tip and its magnetization direction (assumed vertical) were convolved with the ideal (zero tip width) response. Tip widths no greater than the scan height gave acceptable detail in the response curves (Figure 5).

Although the Néel cap eliminates Bloch-wall surface poles, the dominant signal in the simulated MFM profiles over the top surface is symmetric and must be due to the underlying Bloch wall. Even though the Bloch wall does not extend to the surface and produce poles, it generates a surface field with large gradients. There is also an antisymmetric and offset signal due to the Néel cap, but it is only really obvious with a narrow MFM tip scanning close to the surface.

The half-widths of the d^2H_z/dz^2 surface profiles are reasonable estimates of the Bloch wall width, w, for tip widths of 0 and 50 nm (5 cell widths). Too broad a tip results in a complex peak shape from which it is difficult to estimate w. The Néel cap position and width are fairly well determined by using the minima in each profile. Again, too wide a tip degrades the signal so that the Néel cap parameters become difficult to estimate.

Discussion

The cross-sectional structure we have calculated for a 180° wall in magnetite is similar in general aspect to the corresponding structure predicted for iron (Scheinfein et al., 1991). However, the Néel cap is less strongly developed in magnetite. It extends to a depth of ≈0.5w, compared to a depth of ≈w in iron. Another difference is that spins at depth in the Bloch wall deflect slightly out of the wall plane to form a distributed flux return path within the crystal volume.

In iron, the Néel cap extends deeper and $\mathbf{M}_s$ vectors at depth are confined strictly to the Bloch wall plane, so that the flux must close by a loop extending across the crystal to a Néel cap on the opposite face. These differences are accounted for by the greater importance

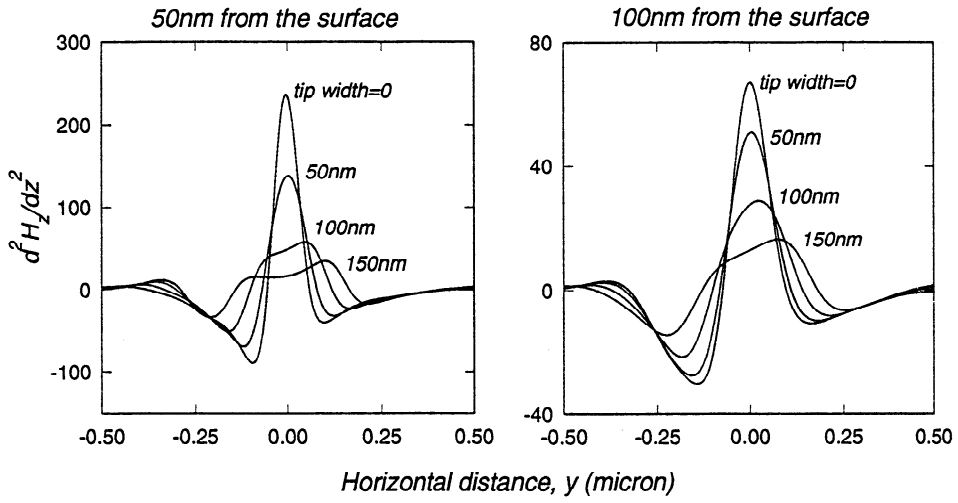

Figure 5. Simulated MFM profiles over the modeled 180° wall, for different MFM tip widths and scan heights (y= 0 corresponds to the center of the Bloch wall at depth). The almost symmetric central peak is due to the underlying Bloch wall. The asymmetry and offset of the flanking negative peaks are due to the Néel cap.

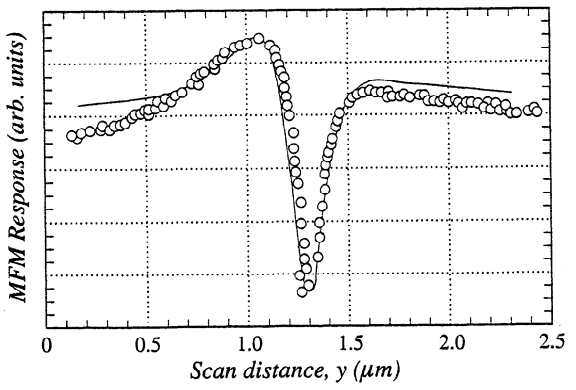

Figure 6. MFM data (circles) measured across a 180° wall in magnetite and the best-fit profile using a simple model (after Proksch et al., 1994). The experimental profile is very similar to our model profile (Figure 5) for similar MFM parameters (the profiles are inverted with respect to each other).

in iron of E_d compared to other energies. For example, $E_d/E_a \propto M_s^2/K_1$ and is thus $(1710/480)^2/(48/12.5) = 3.3$ times larger in iron than in magnetite. The avoidance of poles at the crystal surface (the cause of Néel caps) and on the Bloch wall-domain interface (the cause of in-plane rotation of spins in a Bloch wall) is less imperative in magnetite than in iron. Of course, walls have other ways of reducing E_d which are not taken into account in micromagnetic modeling. One way is through subdivision by Bloch lines into zig-zag segments of alternating magnetic polarity or chirality. Walls should be more finely segmented in iron than in magnetite (Shtrikman and Treves, 1960), and this is observed experimentally (Williams et al., 1992; Proksch et al., 1994).

The first MFM images of domain walls in magnetite were reported by Williams et al. (1992) for a polished {110} surface of a 5-mm natural single crystal. Using a scanning height of 150 nm, symmetric profiles with a single force maximum were obtained across a 180° wall between lamellar domains. The favoured interpretation of the profiles was a zig-zag Bloch wall with surface poles of opposite sign on alternate segments. An asymmetric Bloch wall with an offset Néel cap was not ruled out, but the allowable depth of the Néel cap was only 20 nm, much less than the 70 nm our model predicts.

Proksch et al. (1994) also reported MFM images of domain wall structure on a {110} polished surface of a magnetite single crystal. Their experimental and fitted profiles are reproduced in Figure 6. They used a tip width of 30 nm and a scan height of 110 nm. The surface intersection of the wall was shown to be parallel to <111>, ruling out zig-zag walls.

The measured profile is noticeably asymmetric and (apart from being inverted) is very similar to our predicted profile for a similar tip width and height (Figure 5). In fact, our micromagnetic prediction gives a significantly better fit to Proksch et al.'s data than their theoretical model, in which the Bloch wall was represented by a line of poles 160 nm below the crystal surface and the Néel wall by an offset line of surface dipoles.

The half-width of Proksch et al.'s profile is 210 ± 40 nm. Our predicted half-width for a 50 nm tip 100 nm above the surface is ≈160 nm (Figure 5), which is also the Bloch wall width w predicted in Figure 4. The agreement is reasonable.

Conclusions

1. Near the crystal surface, domain walls are Néel-like: the spins rotate in the plane of the surface.
2. The Néel cap is shallow, approximately one-half the Bloch wall width or 0.07 μm for 180° walls in magnetite.
3. The Néel cap is offset 0.1-0.2 μm with respect to the underlying Bloch wall for 180° walls.
4. As first predicted by LaBonte (1969), the Néel cap forms part of a flux closure loop. However, unlike the situation in films of iron (Scheinfein et al., 1991) and permalloy (Humphrey and Redjdal, 1994), the flux loop closes within the crystal volume and not by linking to another Néel cap on the opposite face.
5. Surface field profiles should be affected by both the volume and the offset of the Néel cap. For MFM tip widths ≤50 nm and scan heights ≤100 nm, the Bloch wall width is well represented by the half-width of the central peak. The Néel cap width and offset can be determined from the spacing and position of the two flanking peaks of opposite sign.
6. Our predictions about Bloch-wall widths and Néel-cap widths and offsets are in reasonable agreement with MFM measurements on magnetite by Proksch et al. (1994). They agree less well with profiles measured by Williams et al. (1992).

Acknowledgments. We thank Sheryl Foss and Bruce Moskowitz for useful discussions, Karl Fabian and an anonymous referee for helpful reviews, and the University of Toronto for use of the KSR1 computer. This research has been suppported by NSERC grant A7709 to D.J.D.

References

Berkov, D.V., K. Ramstöck, and A. Hubert, Solving micromagnetic problems: towards an optimal method, *Phys. Stat. Solidi, (a), 137*, 207-225, 1993.

Fabian, K., A. Kirchner, W. Williams, F. Heider, A. Hubert, and T. Leibl, Three-dimensional micromagnetic calculations for magnetite using FFT, *Geophys. J. Int., 124*, 89-104, 1996.

Humphrey, F.B. and M. Redjdal, Domain wall structure in bulk magnetic material, *J. Magn. Magn. Mat., 133*, 11-15, 1994.

Kittel, C., Physical theory of ferromagnetic domains, *Rev. Mod. Phys., 21*, 541-583, 1949.

LaBonte, A.E., Two-dimensional Bloch-type domain walls in ferromagnetic films, *J. Appl. Phys., 40*, 2450-2458, 1969.

Landau, L.D. and E.M. Lifschitz, On the theory of the dispersion of magnetic permeability in ferromagnetic bodies (transl. from Russian), *Phys. Z. Sowjetunion, 8*, 153-169, 1935.

Lilley, B.A., Energies and widths of domain boundaries in ferromagnetics, *Phil. Mag., 41*, 792-813, 1950.

Néel, L., Les lois de l'aimantation et de la subdivision en domaines élémentaires d'un monocristal de fer, *J. Phys. Radium, 5*, 265-276, 1944.

Néel, L., Remarques sur la théorie des propriétés magnétiques des couches minces et des grains fins, *J. Phys. Radium, 17*, 250-255, 1956.

Newell, A.J., W. Williams, and D.J. Dunlop, A generalization of the demagnetizing tensor for nonuniform magnetization, *J. Geophys. Res., 98*, 9551-9555, 1993.

Özdemir, Ö., S. Xu, and D.J. Dunlop, Closure domains in magnetite, *J. Geophys. Res., 100*, 2193-2209, 1995.

Proksch, R.B., S. Foss, and E.D. Dahlberg, High resolution magnetic force microscopy of domain wall fine structures, *IEEE Trans. Magn., 30*, 4467-4472, 1994.

Scheinfein, M.R., J. Unguris, J.L. Blue, K.J. Coakley, D.T. Pierce, and R.J. Celotta, Micromagnetics of domain walls at surfaces, *Phys. Rev., B, 43*, 3395-3422, 1991.

Sharma, P.V., Rapid computation of magnetic anomalies and demagnetization effects caused by bodies of arbitrary shape, *Pure Appl. Geophys., 64*, 89-109, 1966.

Shtrikman, S. and D. Treves, Fine structure of Bloch walls, *J. Appl. Phys., 31*, 1304, 1960.

Williams, W., V. Hoffmann, F. Heider, T. Göddenhenreich, and C. Heiden, Magnetic force microscopy imaging of domain walls in magnetite, *Geophys. J. Int., 111*, 417-423, 1992.

Xu, S., D.J. Dunlop, and A.J. Newell, Micromagnetic modeling of two-dimensional domain structures in magnetite, *J. Geophys. Res., 99*, 9035-9044, 1994.

Yuan, S.W. and H.N. Bertram, Fast adaptive algorithms for micromagnetics, *IEEE Trans. Magn., 28*, 2031-2036, 1992.

Song Xu and David J. Dunlop, Department of Physics, Erindale College, University of Toronto, 3359 Mississauga Road North, Mississauga, Ontario, Canada L5L 1C6. (e-mail: dunlop@physics.utoronto.ca)

(Received December 14, 1995; revised May 1, 1996; accepted May 13, 1996.)